Beam dynamics and wave packet splitting in a periodically-curved optical waveguide: multimode effects

Beam dynamics and wave packet splitting in a periodically curved optical waveguide: Multimode effects

M. Marangoni, D. Janner, R. Ramponi, P. Laporta, and S. Longhi
Dipartimento di Fisica and Istituto di Fotonica e Nanotecnologie del CNR, Politecnico di Milano, Piazza L. da Vinci 32, I-20133 Milano, Italy

E. Cianci and V. Foglietti
Istituto di Fotonica e Nanotecnologie del CNR, Sezione di Roma, Via Cineto Romano 42, 00156 Roma, Italy
(Received 7 April 2005; published 17 August 2005)

A theoretical and experimental analysis of beam dynamics and wave packet splitting of light in a periodically bent optical waveguide, a phenomenon recently observed [Phys. Rev. Lett. **94**, 073002 (2005)] which is the optical equivalent of adiabatic stabilization of atoms in intense and high-frequency laser fields, is presented in the multimode operational regime. Inhibition of wave packet splitting is theoretically predicted and experimentally observed for higher-order mode excitation.

DOI: 10.1103/PhysRevE.72.026609 PACS number(s): 42.82.Et, 32.80.Rm

I. INTRODUCTION

Optical waveguides with a periodically curved axis have been recently proposed [1] and experimentally demonstrated [2] to provide an experimentally accessible and feasible laboratory tool to study in an optical system the electronic wave packet dynamics of an atom subjected to an intense and high-frequency laser field, a subject which has attracted great theoretical attention for more than two decades despite that the lack of adequate superintense and high-frequency lasers has set severe limits on experimental investigations (for a recent review see [3]). The quantum-optical analogy stems from the equivalence between the semiclassical Schrödinger equation of the electronic wave function of a two-dimensional (2D) atom in an external driving laser field, written in the Kramers-Henneberger (KH) reference frame—the rest frame of a classical electron in the laser field—and the paraxial wave equation for beam propagation in the periodically curved waveguide. The spatial propagation coordinate along the waveguide plays, in the optical system, the same role as the time variable in the laser-atom context, whereas the external driving laser field is simulated by the periodic bending of the waveguide. One of the most interesting dynamical behaviors, first predicted by Pont, Gavrila, and co-workers in the study of atomic hydrogen driven by a high frequency and linearly polarized laser field, is the adiabatic stabilization of the atom [4], which has been commonly associated with a splitting of the ground state hydrogen wave function [5]. In the high-frequency limit, where the electron dynamics cannot follow the fast periodic oscillations of the potential introduced by the laser field, wave packet splitting can be easily understood as due to the dichotomous shape of the cycle-averaged (dressed) atomic potential seen by the electron in the KH reference frame; the electronic wave function can be adiabatically driven from the ground state of atomic hydrogen into the dichotomous shape by a slow turn on of the driving laser pulse. A clear experimental observation of the related wave packet splitting of light in a periodically curved waveguide with adiabatic increase of the axis modulation depth has been recently reported in Ref. [2] and explained on the basis of an adiabatic Y branch splitter within a cycle-averaged waveguide model. Though the adiabatic evolution of the ground-state (fundamental) mode to the final dichotomous pattern was clearly shown in previous works in close connection with similar electron wave packet splitting under a smooth turn on of the laser pulse, the role played by higher-order waveguide modes—corresponding, in the atomic analogy, to excited-state electronic states—has not yet been comprehensively investigated [6], despite that experimental evidence of multimode effects was briefly mentioned in Ref. [2].

In this paper we investigate, both experimentally and theoretically, light beam dynamics in a periodically curved waveguide operating in the multimode regime, and provide experimental evidence of adiabatic stabilization *without splitting* of the light wave packet. Section II presents experimental results on multimode effects observed in a periodically curved lithium-niobate optical waveguide. In Sec. III a theoretical analysis of multimode beam dynamics is presented and used to clarify the experimental results. In particular, it is shown that the observation of adiabatic stabilization without splitting may be related to the adiabatic excitation of a higher-order weakly guided mode of the cycle-averaged waveguide. Finally, in Sec. IV the main conclusions are outlined.

II. MULTIMODE BEAM DYNAMICS IN A PERIODICALLY CURVED OPTICAL WAVEGUIDE: EXPERIMENTAL RESULTS

The waveguide realized for our experiment—previously described in Ref. [2] to study wave packet splitting—consists of a graded-index channel waveguide, with a periodic axis bending (see Fig. 1), fabricated by the annealed proton exchange (APE) technique in z-cut congruent lithium niobate [7].

APE waveguides show positive refractive index change solely for extraordinary wave propagation, so that only TM

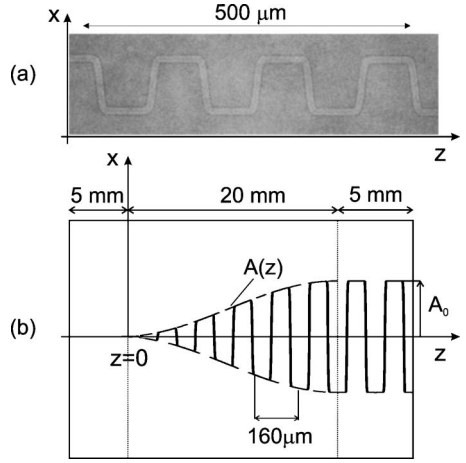

FIG. 1. (a) Microscope image (particular) of the periodically bent lithium niobate waveguide. (b) Schematic of the full waveguide structure, comprising a first section of straight waveguide, an adiabatic section where the waveguide bending amplitude $A(z)$ increases from zero to $A_0=40$ μm, and a final section of periodically curved waveguide with constant bending amplitude.

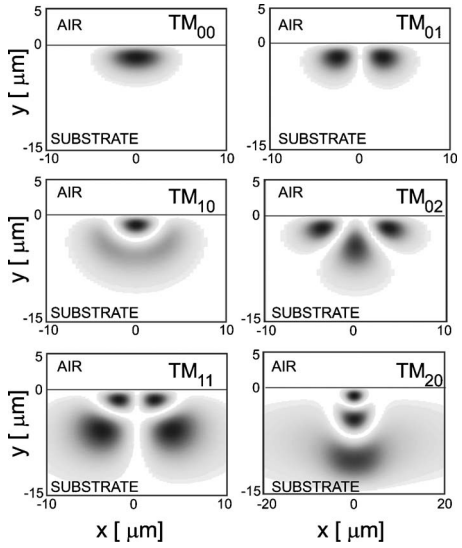

FIG. 2. Numerically computed intensity profiles of the TM guided modes of the channel waveguide at $\lambda=1064$ nm for parameter values which apply for the fabricated lithium-niobate waveguide.

modes are supported by the structure. The waveguide channel width and the refractive index change—for extraordinary TM waves—have been chosen such that the waveguide turns out to be single-mode under 1550-nm-wavelength excitation [2]; however, at 1064 nm wavelength the waveguide is multimode, supporting six TM modes. Specifically, the transverse profile of the waveguide refractive index $n(x,y)$, which results from APE fabrication, can be expressed as $n(x,y)=n_c\simeq 1$ for $y<0$ (in the air) and $n(x,y)=n_s+\Delta n g(x)f(y)$ for $y>0$ (in the substrate), where n_s is the extraordinary refractive index of the substrate, $\Delta n \ll n_s$ is the peak index change, $g(x)=[\mathrm{erf}((x+w)/D_x)-\mathrm{erf}((x-w)/D_x)]/[2\ \mathrm{erf}(w/D_x)]$ and $f(y)=\exp(-y/D_y)$ are, respectively, the refractive index profile parallel and perpendicular to the surface of the waveguide, $2w$ is the channel width, and D_x, D_y are the lateral (x-direction) and in-depth (y-direction) diffusion lengths [8]. For parameter values $w\simeq 5$ μm, $D_x\simeq 2.4$ μm, $D_y\simeq 3.5$ μm, and $n_s\simeq 2.156$, $\Delta n\simeq 0.0145$ (at $\lambda=1064$ nm) which apply to our waveguide, computation of waveguide eigenmodes by a standard finite-difference mode solver method (see Sec. III C for more details) shows that the waveguide can support, at $\lambda=1064$ nm, six TM_{lm} guided modes with $(l,m)=(0,0)$, (0,1), (1,0), (0,2), (1,1), and (2,0), where l and m denote the vertical (y-direction) and horizontal (x-direction) number of zeros in the intensity mode profile, respectively (see Fig. 2).

The z axis of the waveguide is not straight but shows a periodic bending, along the horizontal x direction, with a period $\Lambda=160$ μm and with a nonsinusoidal profile depicted in Fig. 1(a). The amplitude of axis bending is slowly and adiabatically increased from zero to a constant value $A_0=40$ μm by a quarter sine-square envelope $A(z)$, which is shown Fig. 1(b) by a dashed curve. The total length of the waveguide is 30 mm and comprises a 5-mm-long section of straight waveguide, a 20-mm-long adiabatic section in which the amplitude of the bending is increased up to 40 μm, and a final 5-mm-long section of bent waveguide with a constant modulation amplitude. The waveguide was probed at $\lambda=1064$ nm using a single-mode and linearly polarized Nd:YAG laser by focusing its circular diffraction-limited TEM_{00} Gaussian mode into the input face of the waveguide through either a 25× or a 40× microscope objective; the spot size radius of the focused Gaussian laser beam on the input waveguide facet was estimated to be $\simeq 3.2$ μm and $\simeq 2.0$ μm in the two cases, respectively. The polarization of the incident beam was set orthogonal to the plane of the waveguide in order to couple the TM modes supported by the APE waveguide. The transverse light beam distribution at the exit of the waveguide was imaged onto an infrared Vidicon camera (Hamamatsu model C2400-03), with a magnification of $\simeq 25$, and analyzed using beam profiler software. Since the first 5-mm-long straight section of the waveguide is multimode, different patterns at the output waveguide facet were observed depending on the alignment condition of the focusing beam onto the input waveguide channel. Figure 3 shows typical output beam patterns observed and recorded on the Vidicon camera for the two different focusing microscope objectives and for different vertical or horizontal shifts of the focused laser beam with respect to the waveguide channel. The patterns shown in Figs. 3(a) and 3(d) are typically observed using the 25× microscope objective, i.e., with the broader focused beam, the latter pattern being observed when the focused beam is vertically displaced toward the substrate. The pattern shown in Fig. 3(b) can be observed with both the 25× and 40× microscope objectives. Finally, the pattern shown in Fig. 3(c) is observed only under tight focusing (40× microscope objective) with a horizontal displacement of the focused beam from the waveguide channel center. It is clear that, by changing both the size of the focused beam and its vertical or horizontal displacement, different waveguide modes—or a linear combination of them with weights depending on spatial overlapping integrals—are excited in the first straight section of the waveguide, and different intensity patterns are correspondingly observed at

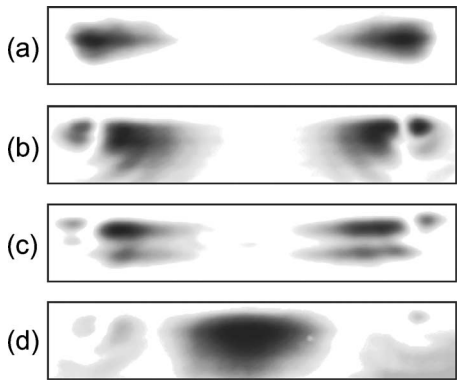

FIG. 3. Recorded intensity patterns of the light beam at the output of the waveguide measured for different focusing conditions (see text). The size of recorded images is 100 μm (horizontal) $\times 20$ μm (vertical).

the output plane. An explanation of the experimental measurements will be given in the next section. Here we limit ourselves to note that, interestingly, the patterns shown in Figs. 3(a)–3(c) lead in any case to a wave packet splitting as expected on the basis of the Y-branch shape for the cycled-averaged potential ([2,5]; see also Fig. 4); conversely, the pattern shown in Fig. 3(d) preferentially localizes light *between* the two potential wells, indicating that adiabatic stabilization can occur without mode splitting. As we will discuss in the next section, such a dynamics may be related to the excitation of a weakly localized mode of a double-well potential, which is a characteristic signature of the multimode regime. In the atomic analogy and within the high-frequency limit [5], the pattern shown in Fig. 3(d) would correspond to a quasistationary higher-order Floquet state for the electronic wave function which is preferentially localized between the two wells of the cycled-average potential and its energy is therefore close to the upper limit for ionization (see Sec. III C and Fig. 7 for more details). In this state the atom is yet adiabatically stabilized by the external field though stabilization does not lead to wave packet splitting.

III. THEORETICAL ANALYSIS

The experimental observations reported in the previous section clearly show that in the multimode regime beam dynamics along the periodically curved waveguide strongly depends on the mode excitation at the input waveguide facet. In order to understand the experimental results and to highlight the key role played by the adiabatic section of the waveguide, a detailed numerical analysis, based on both beam propagation simulations and adiabatic analysis of waveguide eigenmode evolution along the adiabatic section, have been performed. In particular, we will explain the inhibition of wave packet splitting shown in in Fig. 3(d) as due to the excitation of a weakly localized mode of the cycle-averaged waveguide.

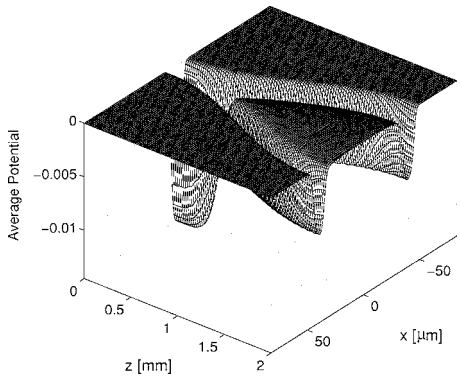

FIG. 4. Behavior of the cycled-averaged potential $V_{av}(x,y,z)$, taken at $y=0^+$, along the adiabatic section of the optical waveguide.

A. Basic equations

Since the fractional power in the air region is very small and the guiding refractive index step Δn is small, light propagation along the waveguide can be well-described by a scalar Helmholtz equation for the electric field amplitude $E(x,y,z)$ (see, for instance, [8]), namely:

$$\frac{\partial^2 E}{\partial z^2} + \nabla_\perp^2 E + k^2 n^2 (x - x_0(z), y) E = 0, \tag{1}$$

where $k=2\pi/\lambda$ is the wave number (in vacuum) of the injected light, $\nabla_\perp^2$ is the transverse Laplacian, and $x_0(z)$ is the axis bending profile. Note that $x_0(z)$ can be expressed by the product of the rapidly varying periodic function $f(z)$, shown in Fig. 1(a), with the slowly varying envelope $A(z)$ shown in Fig. 1(b), i.e., $x_0(z)=A(z)f(z)$. After setting $E(x,y,z) = \psi(x,y,z)\exp(ikn_s z)$ and introducing the paraxial approximation ($|\partial^2\psi/\partial z^2| \ll kn_s|\partial\psi/\partial z|$), from Eq. (1) one obtains for the envelope ψ the following evolution equation:

$$i\lambda\frac{\partial\psi}{\partial z} = -\frac{\lambda^2}{2n_s}\nabla_\perp^2\psi + V(x - x_0(z), y)\psi, \tag{2}$$

where we have set $\lambda \equiv \lambda/(2\pi) = 1/k$ and $V(x,y) \equiv [n_s^2 - n^2(x,y)]/(2n_s) \simeq n_s - n(x,y)$. As previously noted in Refs. [1,2], after the formal substitution $z \to t$, $\lambda \to \hbar$, and $n_s \to m$, Eq. (2) may be viewed as the semiclassical Schrödinger equation, written in the KH reference frame, for a 2D electron in the binding potential $V(x,y)$, subjected to an external field linearly polarized along the x axis. As discussed in Ref. [1], in the high-frequency modulation regime, i.e., for a short modulation period of waveguide bending, the light field cannot follow the rapid longitudinal variation of the refractive index and beam dynamics is governed, at leading order, by a cycled-averaged potential. The high-frequency limit leads to the cycle-averaged wave equation [1]:

$$i\lambda\frac{\partial\psi}{\partial z} = -\frac{\lambda^2}{2n_s}\nabla_\perp^2\psi + V_{av}(x,y,z)\psi, \tag{3}$$

where

$$V_{av}(x,y,z) = \frac{1}{\Lambda}\int_0^\Lambda dz' V(x - A(z)f(z'), y) \tag{4}$$

is the cycled-averaged potential. Note the dependence of V_{av} on z, which comes from the slow ramp envelope $A(z)$ in the adiabatic section of the waveguide. The behavior of the cycled-averaged potential $V_{av}(x,y,z)$ at $y=0^+$ for the fabri-

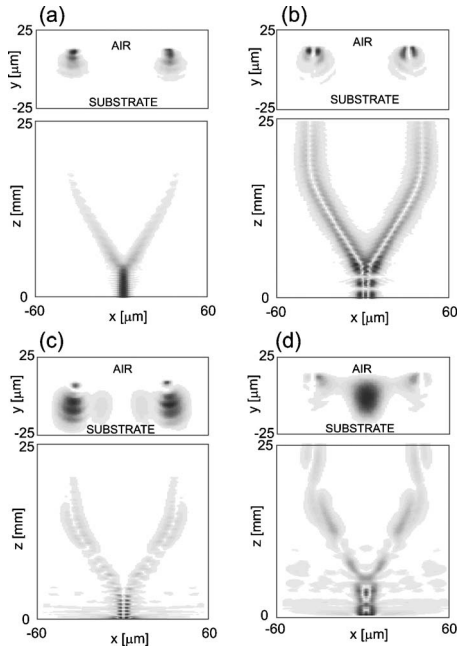

FIG. 5. Numerical simulations showing light propagation along the waveguide at the $y=0$ plane (lower plots) and corresponding intensity patterns at the output plane (upper plots) under different waveguide excitation at the input plane: (a) TM_{00} excitation, (b) TM_{10} excitation, (c) TM_{11} excitation, and (d) TM_{20} excitation.

cated waveguide is depicted in Fig. 4, which clearly corresponds to an adiabatic Y branch waveguide. Though the simplest average waveguide model, given by Eq. (3), may be too crude to fully describe wave dynamics—mainly because it does not account for discrete effects typical of segmented waveguides [9] and neglects radiation losses which are considerable in our experimental conditions [2]—it clearly predicts wave packet splitting as due to the existence of a Y branch. In addition, for an average potential V_{av} slowly varying with propagation distance, in the absence of mode crossing the well-known adiabatic theorem of quantum mechanics [10] can be applied to Eq. (3) to study the beam evolution of a given eigenmode. To explain the experimental patterns shown in Fig. 3, we proceed both by a direct numerical analysis of Eq. (2), using a beam propagation approach, and by invoking the adiabatic theorem calculating the adiabatic evolution of eigenvalues and eigenmodes for the cycled-averaged Schrödinger equation (3).

B. Beam propagation: Numerical results

We numerically integrated Eq. (2) using a standard pseudospectral split-step technique on a rectangular 140 μm $\times 80$ μm integration domain with 256×256 spectral modes. Absorbing boundary conditions were assumed to account for radiation losses induced by waveguide bending [1]. In order to highlight multimode effects on beam splitting dynamics, we performed numerical simulations on beam evolution when the initial straight waveguide is excited, at the input plane, with one of its TM modes (see Fig. 2). Figure 5 shows, as an example, beam evolution (lower plots) and corresponding output intensity patterns (upper plots) as obtained when the waveguide is excited in its TM_{00}, TM_{10}, TM_{11}, and TM_{20} modes. The evolution of beam amplitude $|\psi|$ in the figures as a function of propagation distance z is taken at the air-substrate interface, i.e., at $y=0$. The output intensity patterns shown in Figs. 5(a)–5(c), leading to beam splitting according to the Y-branch averaged potential (see Fig. 4), are similar to the experimental ones reported in Figs. 3(a)–3(c), respectively. Interestingly, waveguide excitation of the TM_{20} mode [Fig. 5(d)] does not lead, as one would expect, to beam splitting as in other cases, instead a broad spot is observed which resembles the one observed in the experiment [compare Fig. 5(d) with Fig. 3(d)]. Note that the evolution of beam amplitude at the air-substrate interface for this case, shown in the lower plot of Fig. 5(d), indicates an apparent beam splitting behavior, which, however, does not occur; this is due to the fact that the broad central lobe, clearly visible in the upper plot of Fig. 5(d), is localized in the substrate region, a few microns below the air-substrate interface. Therefore in the top view, taken at $y=0$ and shown in the lower plot of Fig. 5(d), the broad central spot is not visible. Since the experimental pattern shown in Fig. 3(d) was observed for the broader focusing laser spot vertically displaced from the waveguide channel in the substrate, it is likely that inhibition of beam splitting observed in the experiment is due to excitation of the TM_{20} waveguide mode. This mode, indeed, shows a three-spot pattern (see Fig. 2), with the most intense and broad lobe being localized a few microns below the air-substrate interface.

C. The average waveguide model: Adiabatic analysis

Beam propagation simulations under different waveguide mode excitation (Fig. 5) satisfactorily reproduce the main experimental results, highlighting the role of higher-order modes on beam splitting dynamics. However, the explanation of some of the observed effects, such as inhibition of beam splitting [Figs. 3(d) and 5(d)], is nontrivial and deserves an additional investigation. Further physical insights into the role played by higher-order modes into beam dynamics can be obtained by considering beam propagation in the framework of the cycle-averaged waveguide limit [Eq. (3)]. In this case, the periodically curved waveguide can be simply viewed as a Y-branch waveguide, whose potential $V_{av}(x,y,z)$—shown in Fig. 4—varies slowly with the propagation distance z. Exploiting the adiabatic theorem of quantum mechanics for a slowly varying Hamiltonian [10], one can infer that an initially excited eigenmode of the waveguide adiabatically evolves during propagation following the slow change of the potential, provided that the corresponding eigenvalue curve does not cross other eigenvalues of the Hamiltonian. We numerically computed the 2D eigenmodes and corresponding eigenvalues of the Hamiltonian $\mathcal{H}=-(\lambda^2/2n_s)\nabla_t^2+V_{av}(x,y,z)$, assuming z as a parameter, by discretizing the operator $\mathcal{H}$ on a 160 μm $\times 30$ μm rectangular domain using 400×150 discretization points in the horizontal and vertical directions, respectively. The eigenvalues of $\mathcal{H}$ are then used to evaluate the effective mode indices n_{eff}, which are defined as the mode propagation constants

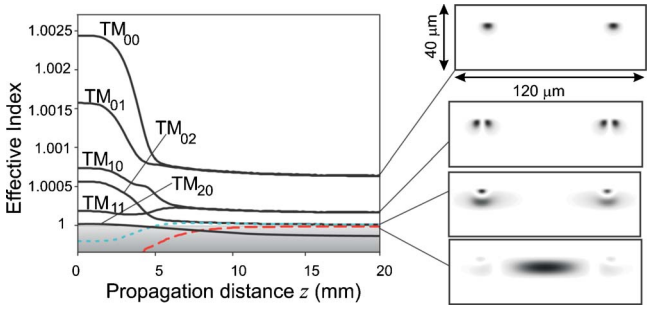

FIG. 6. (Color online) Adiabatic evolution of effective indices for confined (guided) modes of the cycle-averaged Hamiltonian $\mathcal{H}$ vs propagation distance. The dashed curve (in red color) corresponds to the weakly bound mode with antiguiding properties. The shaded area corresponds to unbounded modes (continuous spectrum of $\mathcal{H}$). The dotted curve (in blue color) corresponds to a bound mode emerging from the continuum, which at the end of the waveguide is nearly degenerate with the adiabatically evolved TM_{02} mode.

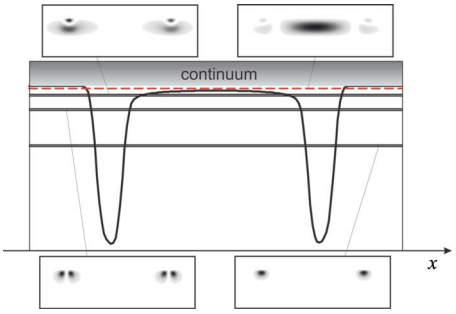

FIG. 7. (Color online) Qualitative behavior of the average potential profile V_{av} vs x (thick solid curve) for $y=0^+$ at the end of the adiabatic waveguide section ($z=20$ mm) and corresponding eigenvalues (energy levels) of the Hamiltonian $\mathcal{H}$ (horizontal lines). The horizontal dashed curve corresponds to the energy level of the weakly guided mode which confines light in between the two potential wells.

normalized to the vacuum wave number k. Figure 6 shows the numerically computed behavior of the effective mode indices versus propagation distance z for bound modes (continuous curves), normalized to the refractive index n_s of the substrate; the shaded area corresponds to the region of radiation modes (continuous spectrum). At $z=0$ there are six guided modes; the intensity mode profiles have been previously shown in Fig. 2, and the modes are accordingly labeled as in Fig. 2. At the end of the adiabatic section, there are seven guided modes, formed by three couples of nearly degenerate modes and by a weakly guided nondegenerate mode (dashed curve, in red color, in Fig. 6). The intensity patterns of such modes are shown in Fig. 6 as well. A few remarks are in order to understand the adiabatic mode evolution shown in Fig. 6 in connection with the experimental and numerical results reported in previous sections.

(i) The lowest-order TM_{00} and TM_{01} modes at $z=0$ adiabatically evolve, without any crossing, towards a couple of nearly degenerate modes after the adiabatic section of the waveguide ($z=20$ mm). Such modes correspond to the usual symmetric and antisymmetric fundamental supermodes of a waveguide coupler [11], both showing a two-spot intensity profile depicted in Fig. 6. Thus excitation of, e.g., the fundamental TM_{00} waveguide mode at $z=0$ leads to adiabatic beam splitting, according to Figs. 3(a) and 5(a) [12].

(ii) Similarly to the previous case, the adiabatic evolution of TM_{10} and TM_{11} modes leads to a couple of nearly degenerate modes at the end of the adiabatic waveguide section, which correspond to symmetric and antisymmetric higher-order supermodes of the splitter. Their intensity profile is shown in Fig. 6 and is qualitatively similar to the patterns shown in Figs. 3(b) and 5(b). Note that the curve for the TM_{10} mode does not show any crossing. In view of the adiabatic theorem, this clearly explains that initial excitation of the waveguide with the TM_{10} mode leads to beam splitting with a two-lobe structure for each splitted spot.

(iii) The curve for the TM_{02} mode and a curve emerging from the continuous spectrum (dotted curve, in blue color, in Fig. 6) adiabatically evolve leading to a couple of nearly degenerate higher-order supermodes of the splitter, whose intensity profile—shown in Fig. 6—qualitatively resembles the patterns observed in Figs. 3(c) and 5(c).

(iv) At the end of the adiabatic section there is a weakly guided mode which emerges from the continuous spectrum (red curve in Fig. 6). Such a mode, whose intensity pattern clearly corresponds to the one observed in Figs. 3(d) and 5(d), is crossed by the curve of mode TM_{20} while falling into the continuum. This crossing may be a way of excitation of such a weakly guided mode and may hence explain the results shown in Figs. 3(d) and 5(d). In practice, different excitation mechanisms, such as excitation of radiation modes induced by waveguide bending and recoupling into the weakly guided mode which deeply extends into the substrate, may be possible as well. It is interesting to observe that, contrary to mode dichotomy characteristic of the other supermodes shown in Fig. 6, the weakly localized mode, marked by the red curve in the figure, confines light *in between* the two wells of the cycle-averaged potential (Fig. 4). Such an antiguiding mechanism can be understood with the help of Fig. 7, where a qualitative energy level diagram of the Hamiltonian $\mathcal{H}$ at the plane $z=20$ mm is plotted along with the profile of the cycle-averaged potential at that plane. From the figure it can be seen that, as the three couples of nearly degenerate symmetric and antisymmetric supermodes have eigenvalues (energy levels) which cross the two wells, the weakly localized mode has an eigenvalue (dashed horizontal line, in red color) which is just below the upper level boundary of continuous modes (ionization) but above the two potential wells.

IV. CONCLUSIONS

In this work we have studied, both experimentally and theoretically, beam dynamics in an optical waveguide with a periodically curved axis, highlighting the important role played by higher-order modes. Such a structure has been recently proposed as an experimentally accessible system to observe the exotic phenomenon of wave packet dichotomy associated with stabilization of atoms in high-frequency and

high-intensity laser fields [2]. In this work we have shown that, in the multimode operational regime, the beam splitting dynamics is more involved and, interestingly, light guiding may occur without any splitting. A detailed numerical analysis, based on both beam propagation simulations and adiabatic mode analysis in the high-frequency limit, has been presented to explain the rather involved scenario observed in the multimode regime.

[1] S. Longhi, D. Janner, M. Marano, and P. Laporta, Phys. Rev. E **67**, 036601 (2003).
[2] S. Longhi, M. Marangoni, D. Janner, R. Ramponi, P. Laporta, E. Cianci, and V. Foglietti, Phys. Rev. Lett. **94**, 073002 (2005).
[3] M. Gavrila, J. Phys. B **35**, R147 (2002).
[4] M. Pont and M. Gavrila, Phys. Rev. Lett. **65**, 2362 (1990).
[5] M. Pont, N. R. Walet, M. Gavrila, and C. W. McCurdy, Phys. Rev. Lett. **61**, 939 (1988).
[6] In a different physical context, adiabatic mode control in unbalanced Y-branch waveguides involving higher-order modes has been previously considered and applied to optical signal processing. See, e.g., H. Yajima, Appl. Phys. Lett. **22**, 647 (1973); J. R. Kurz, J. Huang, X. Xie, T. Saida, and M. M. Fejer, Opt. Lett. **29**, 551 (2004).
[7] M. L. Bortz and M. M. Fejer, Opt. Lett. **16**, 1844 (1991).
[8] A. Sharma and P. Bindal, Opt. Quantum Electron. **24**, 1359 (1992).
[9] Z. Weissman and A. Hardy, J. Lightwave Technol. **11**, 1831 (1993).
[10] See, for instance, A. Messiah, *Quantum Mechanics* (Dover, New York, 1999), p. 744.
[11] See, for instance, A. Yariv, *Optical Electronics*, 4th ed. (Saunders College Publishing, New York, 1991), pp. 519–529.
[12] This is actually the usual scenario encountered if the straight waveguide were single mode. In the single-mode case, typically the adiabatic mode diagram shown in Fig. 6 turns out to show solely two bound modes: one bound mode curve emanates from the fundamental TM_{00} waveguide mode, which adiabatically evolves toward the symmetric supermode of the waveguide splitter at the end of the adiabatic section; the other bound mode emerges from the continuous spectrum and adiabatically evolves toward the antisymmetric supermode of the splitter.